Article

Chinese Science Bulletin

Physical Chemistry

August 2012 Vol.57 No.22: 2901–2907
doi: 10.1007/s11434-012-5260-6

Visible-light photocatalytic activity and mechanism of novel AgBr/BiOBr prepared by deposition-precipitation

LIN HaiLi, CAO Jing*, LUO BangDe, XU BenYan & CHEN ShiFu*

College of Chemistry and Materials Science, Huaibei Normal University, Huaibei 235000, China

Received October 13, 2011; accepted March 6, 2012

A new composite photocatalyst AgBr/BiOBr was prepared by loading AgBr on a BiOBr substrate via deposition-precipitation and characterized by X-ray diffraction, scanning electron microscopy, high-resolution transmission electron microscopy and UV-vis diffuse reflectance spectroscopy. The as-prepared AgBr/BiOBr comprised face-centered cubic AgBr and tetragonal BiOBr particles. The average crystalline sizes of AgBr in the AgBr/BiOBr composites were less than 28.5 nm. The absorption edges of AgBr/BiOBr in visible-light region had a red shift with increasing AgBr content. Photocatalytic degradation of methyl orange results show that the AgBr/BiOBr composites could degrade methyl orange efficiently under visible-light irradiation (λ>420 nm). The optimal molar percentage of AgBr was 50 mol% with corresponding maximum k_{app} of 0.00619 min^{-1}. Active $\cdot O_2^-$ played a major role for methyl orange degradation while h^+ and $\cdot$OH had little effect on the photocatalytic process. The enhancement of photocatalytic activity of AgBr/BiOBr is mainly ascribed to the heterojunction effect between AgBr and BiOBr.

composite photocatalyst, AgBr/BiOBr, deposition-precipitation method, methyl orange, reaction mechanism

Citation: Lin H L, Cao J, Luo B D, et al. Visible-light photocatalytic activity and mechanism of novel AgBr/BiOBr prepared by deposition-precipitation. Chin Sci Bull, 2012, 57: 2901–2907, doi: 10.1007/s11434-012-5260-6

Semiconductor photocatalysis has been widely investigated for its potential application in environmental protection and solar energy transformation. At present, TiO_2 is expected to be one of the most valuable photocatalysts due to its oxidative, chemically stable, economical and non-toxic characteristics [1–4]. However, the restricted visible-light absorption limits its development, which drives us to search for visible-light-induced photocatalysts via two ways, including modification of TiO_2 [5–10] and exploitation of new non-titania-based visible-light photocatalysts [11–14].

BiOX (X=Cl, Br, I) as a significant layer-structured semiconductor has attracted much attention for its visible-light response. Various synthesis methods leading to BiOX have been reported, such as hydrothermal [15–18], transformation from $NaBiO_3$ [19], hydrolysis [20], homogenous deposition [21] and reverse microemulsions [22], which displayed different photoactivities of BiOX. Homogenous deposition is a simple way for the preparation of BiOX that has a plate structure, with high surface area, which facilities the adsorption of dyes and photocatalytic processes. Nowadays, in order to further improve the photoactivity of BiOX, BiOX-based composites have been constructed and adopted, such as BiOI/TiO_2 [23], AgI/BiOI [24], BiOI/Bi_2O_3 [25], $NaBiO_3$/BiOCl [26], Fe_3O_4/BiOCl [27], BiOCl/Bi_2O_3 [28] and WO_3/BiOCl [29]. The synthesis of BiOX-based composites is very important for the development of highly efficient visible light photocatalysts.

AgBr is an important semiconductor widely used as a photosensitive material in photography and as a photocatalyst for the degradation of pollutants or destruction of bacteria [24,30–44]. Compared with BiOBr [18], AgBr [45] has a narrower band gap and higher visible-light absorption. Moreover, the two materials have matching energy band structures, according to the data reported in the literature [18,44], and which can effectively separate photogenerated electrons and holes to achieve enhanced photoactivity

*Corresponding authors (email: caojing@mail.ipc.ac.cn; chshifu@chnu.edu.cn)

relative to that of either AgBr or BiOBr. However, little work has been reported for AgBr/BiOBr [46] heterojunction composites.

Therefore, in this paper, we attempt to prepare a AgBr/BiOBr composite catalyst using a simple deposition-precipitation approach, investigate the photoactivity for the degradation of methyl orange (MO) under visible-light irradiation (λ>420 nm) and ascertain the optimal content of AgBr in AgBr/BiOBr. In addition, the probable reaction mechanism for the degradation of MO with AgBr/BiOBr was studied by exploring the roles of active species and discussing the electrons and holes separation approach in detail.

1 Materials and methods

1.1 Chemicals and materials

All reagents were of analytical purity and were used without further purification. Silver nitrate ($AgNO_3$), sodium bromide (NaBr), bismuth nitrate ($Bi(NO_3)_3\cdot 5H_2O$), ammonia solution, methyl orange (MO), terephthalic acid (TA), benzoquinone (BQ), isopropanol (IPA), ammonium oxalate (AO), sodium hydroxide (NaOH) and glacial acetic acid (HAc) were obtained from Sinopharm Chemical Reagent Co., Ltd, China. Deionized water was used throughout this study.

1.2 Preparation of AgBr/BiOBr photocatalyst

BiOBr was prepared in advance. 1.590 g of $Bi(NO_3)_3\cdot 5H_2O$ was dissolved in 200 mL deionized water and the pH value adjusted to 1.96 with HAc, then 0.339 g of NaBr dissolved in 20 mL deionized water was added to the $Bi(NO_3)_3$ solution dropwise with stirring. After stirring for 30 min, the pH value of the reaction solution was adjusted to 3.0 using ammonia water. The resulting solution was then kept at 85°C with stirring for 12 h. Finally, the BiOBr precipitates were collected, washed and dried at 80°C in air.

AgBr/BiOBr was synthesized by deposition-precipitation. The 1.000 g of BiOBr was dispersed in 100 mL deionized water and sonicated for 20 min. 0.056 g of $AgNO_3$ in 20 mL deionized water was added to the BiOBr suspension with magnetic stirring applied for 30 min. Subsequently 0.034 g of NaBr in 50 mL of deionized water was added dropwise to the mixed solution. The resulting suspension was vigorously stirred for 1 h. Finally the product was filtered, washed with deionized water several times and dried at 65°C for 24 h. AgBr/BiOBr with 10 mol% of AgBr was obtained. Samples with different AgBr contents (from 10 mol% to 60 mol%) were also prepared to investigate the effects of composition on photocatalytic performance.

1.3 Characterization of the AgBr/BiOBr photocatalyst

The powder X-ray diffraction (XRD) analysis of the as-prepared catalyst was carried out with a Bruker D8 Advance X-diffractometer using Cu Kα radiation (λ=1.5406 Å), operated at 40 kV and 30 mA. Scanning electron microscopy (SEM) measurements were recorded on a Sirion200 instrument at a scanning voltage of 5.00 kV. High-resolution transmission electron microscopy (HRTEM) was carried out on a JEOL JEOL-2010 with 200 kV accelerating voltage. The UV-vis diffuse reflectance spectra (DRS) were obtained by a Pgeneral TU-1901 UV-VIS spectrophotometer equipped with an integrating sphere assembly. The analysis range was from 300 to 700 nm and $BaSO_4$ was used as a reflectance standard.

1.4 Photocatalytic activity tests

The photocatalytic activities of AgBr/BiOBr were evaluated by the photodegradation of MO under irradiation of visible-light (λ>420 nm) in a photoreaction apparatus. A 500 W Xe lamp (Institute of Electric Light Source, Beijing, China) was used as the light source with a 420 nm cutoff filter (Instrument Company of Nantong, China) to provide visible-light irradiation. In each experiment, 0.10 g of photocatalyst was added to 50 mL of MO solution (10 mg/L). Prior to illumination, the suspension was magnetically stirred in the dark for 20 min to reach adsorption-desorption equilibrium of MO on the catalyst surface. At irradiation time intervals of 30 min, 5 mL of the suspension was collected, then centrifuged (4000 r/min, 30 min) to remove the photocatalyst particles. The catalyst-free MO solution was analyzed with a 722s spectrophotometer (Shanghai Precision and Scientific Instrument Company, China), with the concentration of MO being determined from its maximum absorption at a wavelength of 464 nm using deionized water as a reference sample.

Experiments to examine the reactions of active species (h^+, $\cdot OH$ and $\cdot O_2^-$) were similar to those used for photodegradation. Different scavengers were introduced into the MO solution prior to the addition of the catalyst. In addition, the terephthalic acid (TA) photoluminescence probe technique was also used in the detection of ·OH radicals. In the detection experiment, a basic TA solution was added to the reactor instead of MO and the concentration of TA was set at 5×10^{-4} mol/L in 2×10^{-3} mol/L NaOH solution. The sample collected every 60 min was measured on a JASCO FP-6500 type fluorescence spectrophotometer after centrifugation, using an excitation wavelength of 315 nm.

2 Results and discussion

2.1 Characterization of AgBr/BiOBr

(i) XRD analysis. Figure 1 shows the XRD patterns of the as-prepared samples. It is observed that all the peaks of the pure AgBr were indexed to (111), (200), (220), (222), (400) and (420) peaks, coinciding with the standard face-centered cubic AgBr phase (JCPDS NO. 06-0438) while (001), (101),

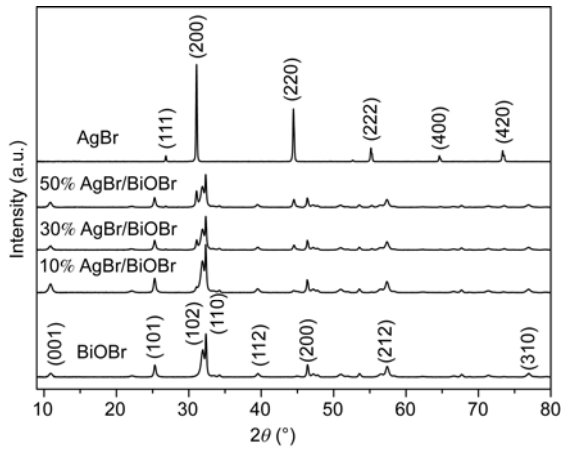

Figure 1 XRD patterns of BiOBr, AgBr/BiOBr and AgBr.

(102), (110), (112), (200), (212) and (310) peaks of BiOBr belonged to tetragonal BiOBr (JCPDS NO. 78-0348), respectively. In addition, the AgBr/BiOBr composite exhibited coexisting phases of AgBr and BiOBr. With increasing amounts of AgBr in AgBr/BiOBr, the peak intensities of AgBr increased gradually while those of BiOBr decreased slightly. The average crystalline sizes of AgBr in the AgBr/BiOBr composites were calculated to be 20.0, 27.0 and 28.5 nm for 10 mol%, 30 mol% and 50 mol% AgBr/BiOBr, respectively, according to the Scherrer formula [47]. Furthermore, no other impurity was detected, which suggests that the AgBr/BiOBr sample is composed only of AgBr and BiOBr.

(ii) SEM and TEM analysis. The SEM images of AgBr/BiOBr (Figure 2) show that the BiOBr substrate comprised a flower-like 3-D aggregate shape with particle sizes of 5–10 μm, as reported elsewhere [17]. The enlarged microstructure displays the lamellar structure of BiOBr. Compared with single BiOBr, the deposited AgBr with irregular shapes on the surface of BiOBr filled in the gaps of the petals, which may facilitate the close contact of AgBr with BiOBr and the efficient transfer of the photoinduced carriers at the AgBr-BiOBr interface.

Figure 3(a) shows that 50% AgBr/BiOBr had an irregular lamellar microstructure. Figure 3(b) displays the HRTEM image of 50% AgBr/BiOBr. The crystal lattice of BiOBr and AgBr can be clearly discerned in the HRTEM image of 50% AgBr/BiOBr. It can be seen that three sets of lattice images are found with d spacings of 0.161 and 0.228 nm, corresponding to the (212) and (122) planes, respectively, of tetragonal BiOBr, while the d spacing of 0.145 nm can be indexed to the (400) plane of AgBr. This result confirms that the AgBr/BiOBr heterojunction was formed in the composite.

(iii) DRS analysis. Figure 4 shows the DRS of the AgBr, BiOBr, and AgBr/BiOBr samples. As can be seen, BiOBr had an absorption edge at about 460 nm, while AgBr had broader absorption in the visible region with an absorption edge of around 505 nm. The absorption edges of AgBr/BiOBr were located in the range of 460–505 nm and had a

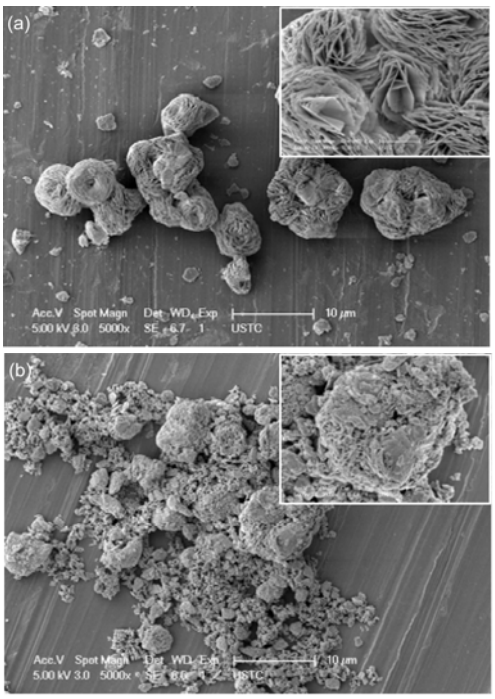

Figure 2 SEM images of BiOBr (a) and 50% AgBr/BiOBr (b).

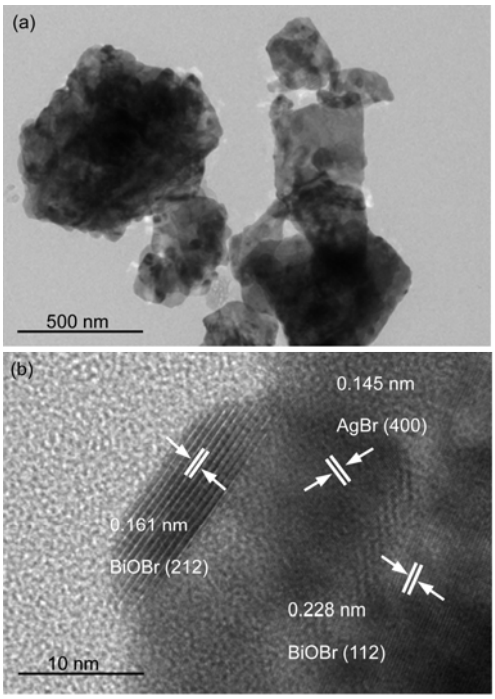

Figure 3 TEM image (a) and HRTEM image (b) of 50% AgBr/BiOBr.

monotonic red shift with increasing AgBr content in the AgBr/BiOBr, which suggests that considerable visible light can be absorbed by AgBr/BiOBr.

Moreover, the band gap energy of a semiconductor can be calculated by eq. (1) [48,49]:

$$\alpha h\nu = A\left(h\nu - E_{\mathrm{g}}\right)^{n/2}, \tag{1}$$

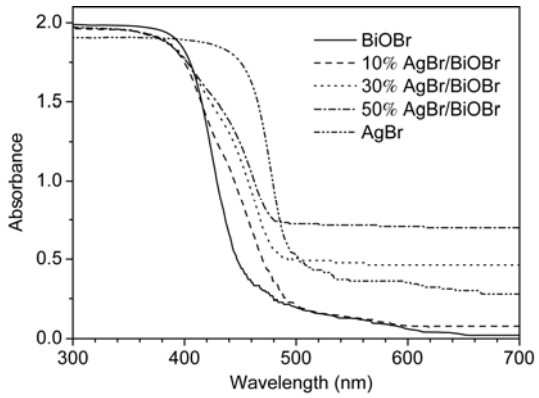

Figure 4 DRS of AgBr, AgBr/BiOBr and BiOBr.

where α, h, v, E_g and A are the absorption coefficient, the Planck constant, light frequency, band gap energy, and a constant, respectively. Among them, n is determined by the type of optical transition of a semiconductor. The value of n for BiOBr is taken as 4, and also for AgBr, due to their indirect transition characteristics. Therefore, the E_g values of BiOBr and AgBr can be determined from a plot of $(\alpha hv)^{1/2}$ versus energy (hv), as shown in Figure 5, and were found to be 2.60 and 2.39 eV, respectively.

In addition, the valence band (VB) and conduction band (CB) edge position of a semiconductor can be estimated according to the following formulae [21]:

$$E_{VB} = X - E^e + 0.5E_g, \tag{2}$$

$$E_{CB} = E_{VB} - E_g, \tag{3}$$

where E_{VB} is the VB edge potential, X is the electronegativity of the semiconductor, which is the geometric mean of the electronegativity of the constituent atoms, E^e is the energy of free electrons on the hydrogen scale (about 4.5 eV). Therefore, the E_{VB} of BiOBr and AgBr were calculated as 2.98 and 2.50 eV, respectively. Thus, the E_{CB} of BiOBr and AgBr were estimated to be 0.38 and 0.11 eV, separately. Therefore, BiOBr and AgBr had matching band potentials, which facilitated the separation of photogenerated electrons and holes.

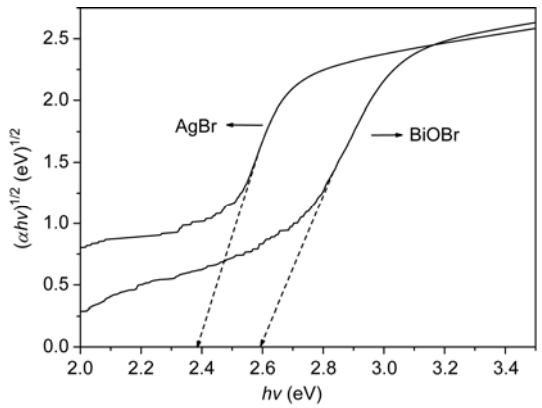

Figure 5 Plot of $(\alpha hv)^{1/2}$ versus energy (hv) for the band gap energies of AgBr and BiOBr.

2.2 Photocatalytic activity of AgBr/BiOBr photocatalyst

The photocatalytic activities of as-prepared samples were evaluated by the degradation of MO under visible-light irradiation. Figure 6 reveals that pure BiOBr had weak photocatalytic activity after 180 min irradiation whereas AgBr/BiOBr presented a higher photocatalytic activity for the degradation of MO under visible-light irradiation. The degradation efficiency of MO increased quickly until the AgBr content rose to 50% and then decreased, which suggests that optimal AgBr content was 50% in AgBr/BiOBr. The photocatalytic activity of AgBr/BiOBr changed with AgBr content can mainly attribute to the role of heterojunction formed between AgBr and BiOBr. When the AgBr content is low, the amount of AgBr/BiOBr heterojunction is not sufficient to separate the photogenerated electrons and holes, which leads to a slow increase in photocatalytic activity, while in the case of excessive AgBr content, the dispersion of AgBr became worse, and the interfaces and heterojunction structures between AgBr and BiOBr particles decreased. As a result, the interfacial charge transfer was suppressed and the photocatalytic activity was lowered. In addition, the increase of AgBr content effectively improved the utilization of visible light, which raised the photocatalytic activity of AgBr/BiOBr. On the base of the synergetic effect of heterojunction and light absorption, 50% AgBr/BiOBr exhibits the best photocatalytic activity for MO degradation.

Based on the Langmuir-Hinshelwood (L-H) kinetics model [48,50–52], the photocatalytic process of MO can be expressed as [50]

$$\ln\left(C_0/C\right) = k_{app}t, \tag{4}$$

where k_{app} is the apparent pseudo-first-order rate constant (min^{-1}), C is the MO concentration in aqueous solution at time t (mg/L) and C_0 is the initial MO concentration (mg/L). The maximum k_{app} of MO degradation was 0.00619 min^{-1},

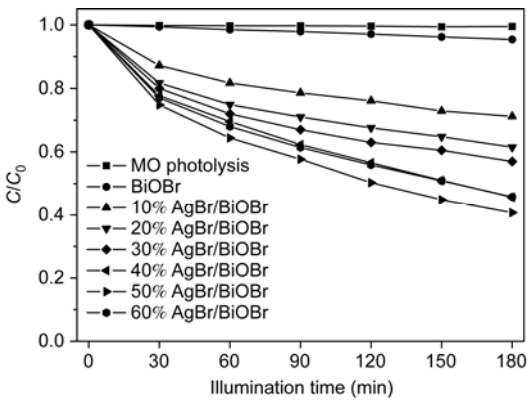

Figure 6 Effect of AgBr content on the degradation efficiency of MO.

obtained over the 50% AgBr/BiOBr photocatalyst.

In order to display the combined role of AgBr/BiOBr for the enhancement of photocatalytic activities, comparative photocatalytic experiments were also carried out using different photocatalysts with the same mass of active component, such as BiOBr and AgBr. Figure 7 shows that the corresponding values of k_{app} for MO degradation were 0.00025, 0.00372 and 0.00619 min^{-1} for BiOBr, AgBr and 50% AgBr/BiOBr, respectively. Furthermore, the photocatalytic activity of AgBr/BiOBr was obviously higher than that of the sum of AgBr and BiOBr, which further emphasizes the role of the heterojunction between AgBr and BiOBr.

The repeated tests (Figure 8) were accomplished and showed that the photocatalytic activity of AgBr/BiOBr obviously declined. The used catalyst became a little darker than the fresh catalyst, which indicates that metallic silver was formed in the used AgBr/BiOBr. This phenomenon has also been observed in previous studies [34,38,39]. The XRD pattern of used AgBr/BiOBr (inset of Figure 8) shows that the crystal structures of AgBr and BiOBr are well maintained and no silver peaks are found at 38.16° and 44.07°. However, the trace amount of silver formed has affected the photocatalytic activity of AgBr/BiOBr. Further experiments should be executed to improve the stability of AgBr/BiOBr. For example, the decrease in the grain size of AgBr may facilitate the transfer of electrons and holes to the surface of AgBr, which will reduce the reaction probability between electrons and interstitial silver ions.

2.3 Possible photocatalytic mechanism

In the photocatalytic oxidation (PCO) process, electron-hole pairs are directly produced by photocatalyst after illumination. Subsequently, a series of photoinduced main active species including h^+, ·OH and $\cdot O_2^-$ are suspected to be involved in the photocatalytic reaction. At present, different ways have been developed to detect these active species. In general, terephthalic acid (TA) combined with photoluminescence (PL) technique can be used as a molecular probe to detect ·OH radicals. The PL emission spectra excited at 315 nm from TA solution were measured every 60 min of illumination and the results are shown in Figure 9. It can be seen that no PL signal at about 425 nm was observed with increasing irradiation time, which demonstrates that no ·OH radicals were formed during the PCO process and confirms that ·OH radicals are not the dominant active species.

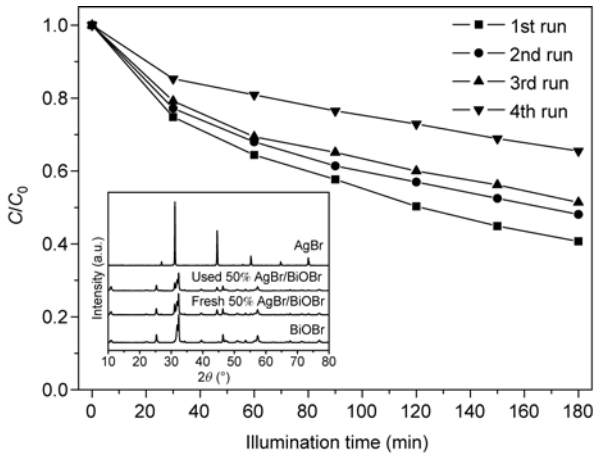

Figure 8 Stability of AgBr/BiOBr for the degradation of MO. Inset: comparison of XRD patterns of fresh and used 50% AgBr/BiOBr.

In order to further evaluate the effect of the other active species, a series of quenchers were introduced to scavenge the relevant active species. As an ·OH scavenger, isopropanol (IPA) was added to the reaction system [39], ammonium oxalate (AO) was introduced as the scavenger of h^+ [53] and benzoquinone (BQ) was adopted to quench $\cdot O_2^-$ [39]. The concentration of scavengers used in this study was 0.1 mmol/L. Control experiment was carried out without quenchers under otherwise identical conditions.

The results of MO degradation efficiencies found with different quenchers are shown in Figure 10. AO and IPA did not obviously affect the k_{app} of MO degradation throughout the experiments, which demonstrates that h^+, as well as ·OH, are not the active species involved in the PCO process. However, after the addition of BQ, the k_{app} decreased

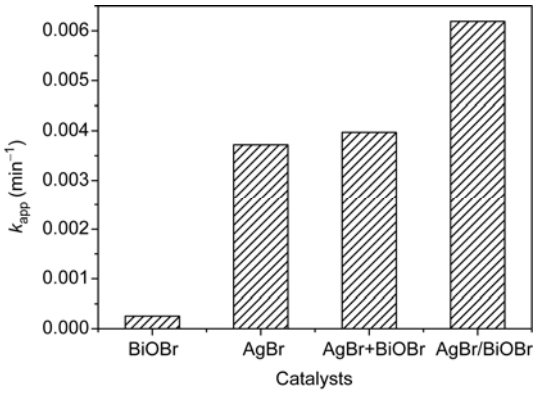

Figure 7 Effect of the combined role of AgBr and BiOBr on the k_{app} of MO.

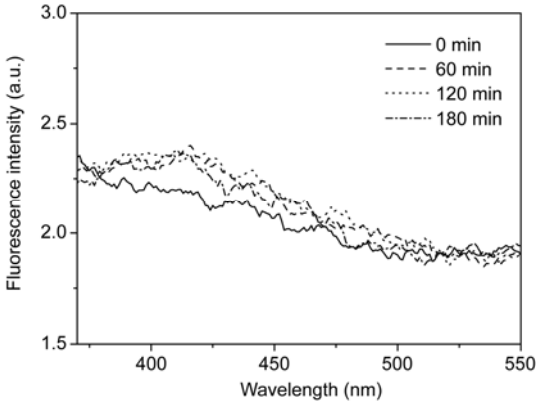

Figure 9 ·OH trapping PL spectral changes observed during irradiation of AgBr/BiOBr in TA solution (excitation at 315 nm).

markedly, which shows that $\cdot O_2^-$ is the dominating active species for AgBr/BiOBr system. The generation of $\cdot O_2^-$ may be via a photogenerated electron reacting directly with O_2 adsorbed on the surface of the catalyst AgBr/ BiOBr.

Based on the band gap structure of as-prepared AgBr/ BiOBr and the effects of scavengers, a possible pathway for the enhancement of photocatalytic activity of AgBr/BiOBr and photocatalytic degradation of MO was proposed as follows (Figure 11): under visible-light irradiation (λ>420 nm), both AgBr and BiOBr can be simultaneously excited to form electron-hole pairs. Subsequently, photogenerated electrons transfer from the CB bottom of AgBr to that of BiOBr. At the same time, photogenerated holes move in the opposite direction from the VB top of BiOBr to that of AgBr. Through this process electron-hole pairs can be separated efficiently, which may improve the photocatalytic activity of AgBr/ BiOBr. After that, electrons accumulated on the side of BiOBr react with O_2 adsorbed on the surface of catalyst to generate reactive $\cdot O_2^-$ that finally leads to the degradation of MO.

It is noted that the calculated VB potential of AgBr (2.50 eV) is more positive than the standard reduction potential of $\cdot OH/OH^-$ (2.38 eV) [24], but this result suggests that $\cdot OH$ radical is not the key factor for the photocatalytic degradation of MO. Since the VB potential of AgBr is just around the $\cdot OH/OH^-$ standard reduction potential, considering the calculation method error of 0.2 eV [54,55], it appears that the over-potential is too small to oxidize OH^- into $\cdot OH$ radical kinetically. In addition, the energy band matching of AgBr and BiOBr is the premise for the enhancement of AgBr/BiOBr, while the effect of the structure of the photocatalyst, such as crystalline structure, electron structure and surface structure, on the photocatalytic activity of AgBr/BiOBr needs to be investigated further.

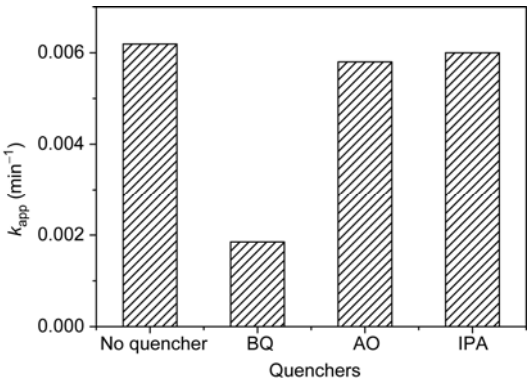

Figure 10 k_{app} values of AgBr/BiOBr with different quenchers.

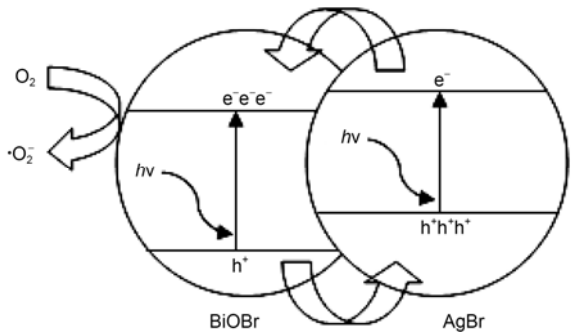

Figure 11 Separation mechanism of photogenerated electrons and holes over AgBr/BiOBr under visible-light irradiation.

3 Conclusions

AgBr/BiOBr was synthesized using a facile deposition-precipitation method. The as-prepared AgBr/BiOBr exhibited good performance for the degradation of MO and displayed much higher photocatalytic activity than either AgBr or BiOBr under visible-light irradiation (λ>420 nm). The maximum k_{app} of 0.00619 min^{-1} for the degradation of MO was obtained when the AgBr content was 50%. Photocatalytic mechanism investigations demonstrate that the degradation of MO over the as-prepared AgBr/BiOBr under visible-light irradiation proceeds mainly via an $\cdot O_2^-$ oxidation process. It may be a promising and efficient photocatalyst for environmental purification applications. The heterojunction formed between AgBr and BiOBr effectively separated the photogenerated electrons and holes, and further improved the photocatalytic activity of AgBr/BiOBr.

This work was supported by the National Natural Science Foundation of China (20973071, 51172086), Natural Science Foundation of Educational Committee of Anhui Province (2012Z356) and Youth Foundation of Huaibei Normal University (2011xqxm31).

1 Inumaru K, Murashima M, Kasahara T, et al. Enhanced photocatalytic decomposition of 4-nonylphenol by surface-organografted TiO_2: A combination of molecular selective adsorption and photocatalysis. Appl Catal B: Environ, 2004, 52: 275–280
2 Yamazakia S, Moria T, Katoua T, et al. Photocatalytic degradation of 4-tert-octylphenol in water and the effect of peroxydisulfate as additives. J Photochem Photobiol A: Chem, 2008, 199: 330–335
3 Tsai W T, Lee M K, Su T Y, et al. Photodegradation of bisphenol-A in a batch TiO_2 suspension reactor. J Hazard Mater, 2009, 168: 269–275
4 Wang R, Ren D, Xia S, et al. Photocatalytic degradation of bisphenol A (BPA) using immobilized TiO_2 and UV illumination in a horizontal circulating bed photocatalytic reactor (HCBPR). J Hazard Mater, 2009, 169: 926–932
5 Zhao W, Ma W H, Chen C C, et al. Efficient degradation of toxic organic pollutants with $Ni_2O_3/TiO_{2-x}B_x$ under visible irradiation. J Am Chem Soc, 2004, 126: 4782–4783
6 Yu J C, Ho W K, Yu J G, et al. Efficient visible-light-induced photocatalytic disinfection on sulfur-doped nanocrystalline titania. Environ Sci Technol, 2005, 39: 1175–1179
7 Ho W, Yu J C, Lee S C. Low-temperature hydrothermal synthesis of S-doped TiO_2 with visible light photocatalytic activity. J Solid State Chem, 2006, 179: 1171–1176
8 Sun Q, Xu Y M. Sensitization of TiO_2 with aluminum phthalocyanine: Factors influencing the efficiency for chlorophenol degradation in water under visible light. J Phys Chem C, 2009, 113: 12387–12394
9 Arabatzis I M, Stergiopoulos T, Bernard M C, et al. Silver modified titanium dioxide thin films for efficient photodegradation of methyl orange. Appl Catal B: Environ, 2003, 42: 187–201
10 Ishibai Y, Sato J, Nishikawa T, et al. Synthesis of visible-light active

TiO_2 photocatalyst with Pt-modification: Role of TiO_2 substrate for high photocatalytic activity. Appl Catal B: Environ, 2008, 79: 117–121
11 Li G S, Zhang D Q, Yu J C. Ordered mesoporous $BiVO_4$ through anocasting: A superior visible light-driven photocatalyst. Chem Mater, 2008, 20: 3983–3992
12 Tang J W, Zou Z G, Ye J H. Effects of substituting Sr^{2+} and Ba^{2+} for Ca^{2+} on the structural properties and photocatalytic behaviors of $CaIn_2O_4$. Chem Mater, 2004, 16: 1644–1649
13 Yamasita D, Takata T, Hara M, et al. Recent progress of visible-light-driven heterogeneous photocatalysts for overall water splitting. Solid State Ionics, 2004, 172: 591–595
14 Shi R, Lin J, Wang Y J, et al. Visible-light photocatalytic degradation of $BiTaO_4$ photocatalyst and mechanism of photocorrosion suppression. J Phys Chem C, 2010, 114: 6472–6477
15 Shang M, Wang W Z, Zhang L. Preparation of BiOBr lamellar structure with high photocatalytic activity by CTAB as Br source and template. J Hazard Mater, 2009, 167: 803–809
16 Zhang J, Shi F J, Lin J, et al. Self-assembled 3-D architectures of BiOBr as a visible light-driven photocatalyst. Chem Mater, 2008, 20: 2937–2941
17 Zhang X, Ai Z H, Jia F L, et al. Generalized one-pot synthesis, characterization and photocatalytic activity of hierarchical BiOX (X=Cl, Br, I) nanoplate microspheres. J Phys Chem C, 2008, 112: 747–753
18 Jiang Z, Yang F, Yang G D, et al. The hydrothermal synthesis of BiOBr flakes for visible-light-responsive photocatalytic degradation of methyl orange. J Photochem Photobiol A: Chem, 2010, 212: 8–13
19 Chang X F, Huang J, Cheng C, et al. BiOX (X=Cl, Br, I) photocatalysts prepared using $NaBiO_3$ as the Bi source: Characterization and catalytic performance. Catal Commun, 2010, 11: 460–464
20 An H Z, Du Y, Wang T M, et al. Photocatalytic properties of BiOX (X=Cl, Br, and I). Rare Metals, 2008, 27: 243–250
21 Wang W D, Huang F Q, Lin X P, et al. Visible-light-responsive photocatalysts *x*BiOBr-(1–*x*)BiOI. Catal Commun, 2008, 9: 8–12
22 Henle J, Simon P, Frenzel A, et al. Nanosized BiOX (X=Cl, Br, I) particles synthesized in reverse microemulsions. Chem Mater, 2007, 19: 366–373
23 Zhang X, Zhang L Z, Xie T F, et al. Low-temperature synthesis and high visible-light-induced photocatalytic activity of BiOI/TiO_2 heterostructures. J Phys Chem C, 2009, 113: 7371–7378
24 Cheng H F, Huang B B, Dai Y, et al. One-step synthesis of the nanostructured AgI/BiOI composites with highly enhanced visible-light photocatalytic performances. Langmuir, 2010, 26: 6618–6624
25 Li Y Y, Wang J S, Yao H C, et al. Chemical etching preparation of BiOI/Bi_2O_3 heterostructures with enhanced photocatalytic activities. Catal Commun, 2011, 12: 660–664
26 Chang X F, Yu G, Huang J, et al. Enhancement of photocatalytic activity over $NaBiO_3$/BiOCl composite prepared by an *in situ* formation strategy. Catal Today, 2010, 153: 193–199
27 Zhang L, Wang W Z, Zhou L, et al. Fe_3O_4 coupled BiOCl: A highly efficient magnetic photocatalyst. Appl Catal B: Environ, 2009, 90: 458–462
28 Chai S Y, Kim Y J, Jung M H, et al. Heterojunctioned BiOCl/Bi_2O_3, a new visible light photocatalyst. J Catal, 2009, 262: 144–149
29 Shamaila S, Sajjad A K L, Chen F, et al. WO_3/BiOCl, a novel heterojunction as visible light photocatalyst. J Colloid Interface Sci, 2011, 356: 465–472
30 Kakuta N, Goto N, Ohkita H, et al. Silver bromide as a photocatalyst for hydrogen generation from CH_3OH/H_2O solution. J Phys Chem B, 1999, 103: 517–519
31 Hu C, Lan Y Q, Qu J H, et al. Ag/AgBr/TiO_2 visible light photocatalyst for destruction of azodyes and bacteria. J Phys Chem B, 2006, 110: 4066–4072
32 Lan Y Q, Hu C, Hu X X, et al. Efficient destruction of pathogenic bacteria with AgBr/TiO_2 under visible light irradiation. Appl Catal B: Environ, 2007, 73: 354–360
33 Elahifard M R, Rahimnejad S, Haghighi S, et al. Apatite-coated Ag/AgBr/TiO_2 visible-light photocatalyst for destruction of bacteria. J Am Chem Soc, 2007, 129: 9552–9553
34 Zang Y J, Ramin F. Photocatalytic activity of AgBr/TiO_2 in water under simulated sunlight irradiation. Appl Catal B: Environ, 2008, 79: 334–340
35 Pourahmad A, Sohrabnezhad S, Kashefian E. AgBr/nanoAlMCM-41 visible light photocatalyst for degradation of methylene blue dye. Spectrochim Acta Part A, 2010, 77: 1108–1114
36 Zhou X F, Hu C, Hu X X, et al. Plasmon-assited degradation of toxic pollutions with Ag-AgBr/Al_2O_3 under visible-light irradiation. J Phys Chem C, 2010, 114: 2746–2750
37 Rodrigues S, Uma S, Martyanov I N, et al. AgBr/Al-MCM-41 visible-light photocatalyst for gas-phase decomposition of CH_3CHO. J Catal, 2005, 233: 405–410
38 Zang Y J, Farnood R, Currie J. Photocatalytic activities of AgBr/Y-zeolite in water under visible light irradiation. Chem Eng Sci, 2009, 64: 2881–2886
39 Li G T, Wong H K, Zhang X W, et al. Degradation of acid orange 7 using magnetic AgBr under visible light: The roles of oxidizing species. Chemosphere, 2009, 76: 1185–1191
40 Wang P, Huang B B, Qin X Y, et al. Ag/AgBr/$WO_3 \cdot H_2O$: Visible-light photocatalyst for bacteria destruction. Inorg Chem, 2009, 48: 10697– 10702
41 Zhang L S, Wong K H, Chen Z G, et al. AgBr-Ag-Br_2WO_6 nanojunction system: A novel and efficient photocatalyst with double visible-light active components. Appl Catal A: Gen, 2009, 363: 211–229
42 Zhang L S, Wong K H, Yip H Y, et al. Effective photocatalytic disinfection of *E. coli* K-12 using AgBr-Ag-Bi_2WO_6 nanojunction system irradiated by visible light: The role of diffusing hydroxyl radicals. Environ Sci Technol, 2010, 44: 1392–1398
43 Asi M A, He C, Su M H, et al. Photocatalytic reduction of CO_2 to hydrocarbons using AgBr/TiO_2 nanocomposites under visible light. Catal Today, 2011, 175: 256–263
44 Cao J, Luo B D, Lin H L, et al. Photocatalytic activity of novel AgBr/WO_3 composite photocatalyst under visible light irradiation for methyl orange degradation. J Hazard Mater, 2011, 190: 700–706
45 Victora R H. Calculated electronic structure of silver halide crystals. Phys Rev B, 1997, 56: 4417–4421
46 Cheng H F, Huang B B, Wang P, et al. *In situ* ion exchange synthesis of the novel Ag/AgBr/BiOBr hybrid with highly efficient decontamination of pollutants. Chem Commun, 2011, 47: 7054–7056
47 Galceran M, Pujol M C, Zaldo C, et al. Synthesis, structural, and optical properties in monoclinic Er:KYb$(WO_4)_2$ nanocrystals. J Phys Chem C, 2009, 113: 15497–15506
48 Jiang R, Zhu H Y, Li X D, et al. Visible light photocatalytic decolourization of C. I. Acid Red 66 by chitosan capped CdS composite nanoparticles. Chem Eng J, 2009, 152: 537–542
49 Dong X, Ding W, Zhang X, et al. Mechanism and kinetics model of degradation of synthetic dyes by UV-vis/H_2O_2/Freeioxallate complexes. Dye Pigments, 2007, 74: 470–476
50 Li Y, Li X, Li J, et al. Photocatalytic degradation of methyl orange by TiO_2-coated activated carbon and kinetic study. Water Res, 2006, 40: 1119–1126
51 Sun J H, Wang X L, Sun J Y, et al. Photocatalytic degradation and kinetics of Orange G using nano-sized Sn(IV)/TiO_2/AC photocatalyst. J Mol Catal A: Chem, 2006, 260: 241–246
52 Wu C, Chang H, Chen J. Basic dye decomposition kinetics in a photocatalytic slurry reactor. J Hazard Mater, 2006, 137: 336–343
53 Zhang N, Liu S Q, Fu X Z, et al. Synthesis of M@TiO_2 (M=Au, Pd, Pt) core-shell nanocomposites with tunable photoreactivity. J Phys Chem C, 2011, 115: 9136–9145
54 Butler M A, Ginley D S. Prediction of flatband potentials at semiconductor-electrolyte interfaces from atomic electronegativities. J Electrochem Soc, 1978, 125: 228–232
55 Chang X F, Huang J, Tan Q Y, et al. Photocatalytic degradation of PCP-Na over BiOI nanosheets under simulated sunlight irradiation. Catal Commun, 2009, 10: 1957–1961